molecular pharmaceutics

pubs.acs.org/molecularpharmaceutics

Article

Para- and Transcellular Transport Kinetics of Nanoparticles across Lymphatic Endothelial Cells

Jacob McCright, Jenny Yarmovsky, and Katharina Maisel*

Cite This: https://doi.org/10.1021/acs.molpharmaceut.3c00720

Read Online

ACCESS | Metrics & More | Article Recommendations | SI Supporting Information

ABSTRACT: Lymphatic vessels have received significant attention as drug delivery targets, as they shuttle materials from peripheral tissues to the lymph nodes, where adaptive immunity is formed. Delivery of immune modulatory materials to the lymph nodes via lymphatic vessels has been shown to enhance their efficacy and also improve the bioavailability of drugs when delivered to intestinal lymphatic vessels. In this study, we generated a three-compartment model of a lymphatic vessel with a set of kinematic differential equations to describe the transport of nanoparticles from the surrounding tissues into lymphatic vessels. We used previously published data and collected additional experimental parameters, including the transport efficiency of nanoparticles over time, and also examined how nanoparticle formulation affected the cellular transport mechanisms using small molecule inhibitors. These experimental data were incorporated into a system of kinematic differential equations, and nonlinear, least-squares curve fitting algorithms were employed to extrapolate transport coefficients within our model. The subsequent computational framework produced some of the first parameters to describe transport kinetics across lymphatic endothelial cells and allowed for the quantitative analysis of the driving mechanisms of transport into lymphatic vessels. Our model indicates that transcellular mechanisms, such as micro- and macropinocytosis, drive transport into lymphatics. This information is crucial to further design strategies that will modulate lymphatic transport for drug delivery, particularly in diseases like lymphedema, where normal lymphatic functions are impaired.

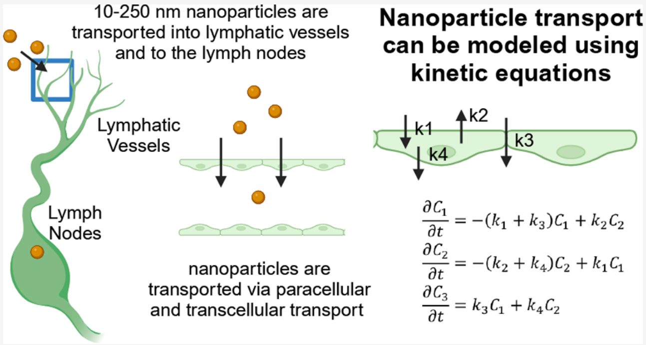

KEYWORDS: *lymphatic endothelial cells (LECs), surface chemistry, micropinocytosis, macropinocytosis, endocytosis, immunotherapy*

■ INTRODUCTION

Nanoparticle-based drug delivery has received significant attention in past decades, culminating in the recent COVID-19 lipid nanoparticle-based RNA vaccines. Nanoparticles provide several advantages to free drug formulations: they can increase drug stability[1] and load,[2] be targeted to specific tissues or cells,[3] and facilitate sustained release of drugs from the nanoparticle core.[4] To enter the relevant cellular compartments, nanoparticles are required to be transported across various biological barriers, including cell monolayers at the intestinal epithelium or blood and lymphatic endothelium, for example. Nanoparticle transport across these cellular barriers occurs via paracellular or transcellular transport mechanisms. Transcellular transport mechanisms include micropinocytosis, macropinocytosis, and/or exocytosis on both sides of the cell layer (Figure 1A), often with concentration gradients driving the dominant direction of the transport. Nanoparticle transport across cellular barriers can be modeled using systems of differential equations utilizing kinetic theories also applied to pharmacokinetic models.[5] A complex system of equations can be used to define the contributions of the individual transport mechanism to the overall transport of

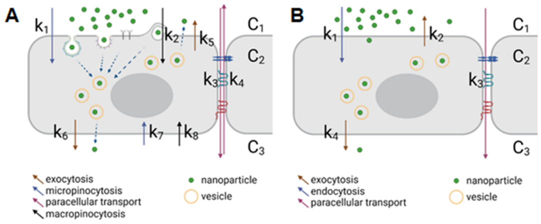

Figure 1. Cellular mechanisms used to transport nanoparticles across cell barriers such as epithelial surfaces and vessel walls. (A) Complex transport considering all potential variables and (B) simplified transport considering only endocytosis, paracellular transport, and exocytosis. Concentrations depict each compartment with C_1 = nanoparticle-rich compartment, C_2 = intracellular compartment, and C_3 = nanoparticle-poor compartment. Full arrows and associated k values represent the kinetics of exocytosis (brown), micropinocytosis (blue), macropinocytosis (black), and paracellular transport (pink).

Received: August 8, 2023
Revised: October 5, 2023
Accepted: October 6, 2023

nanoparticles (eqs 1−3). In these equations, C_1 indicates concentration in the interstitial tissue space, C_2 indicates concentration in the intracellular space, and C_3 indicates concentration in the lumenal space. The rate constants corresponding to transport mechanisms are as follows: k_1: micropinocytosis uptake, k_2: macropinocytosis uptake, k_3: paracellular transport into the vessel, k_4: paracellular transport from the vessel into interstitial space, k_5: exocytosis into interstitial spaces, k_6: exocytosis into the vessel, k_7: micropinocytosis uptake at the lumenal interface, and k_8: macropinocytosis uptake at the lumenal interface. This system of equations can be applied for transport across any system of single-cell layers or other three-compartment models.

$$\frac{\partial C_1}{\partial t} = -(k_1 + k_2 + k_3)C_1 + k_4C_3 + k_5C_2 \tag{1}$$

$$\frac{\partial C_2}{\partial t} = -\,(k_5 + k_6)C_2 + (k_1 + k_2)C_1 + (k_7 + k_8)C_3 \tag{2}$$

$$\frac{\partial C_3}{\partial t} = -\,(k_4 + k_7 + k_8)C_3 + k_6C_2 + k_3C_1 \tag{3}$$

Lymphatic vessel-targeted drug delivery has received significant attention in recent years because lymphatic vessels transport nanoparticle-sized materials from the peripheral tissue to the draining lymph nodes, where the adaptive immune response is shaped. Delivering therapeutics that modulate the immune response directly to the lymph nodes has been shown to enhance their efficacy. Nanoparticles 10−250 nm in size have been shown to be preferentially transported by lymphatic vessels and will accumulate effectively in the lymph nodes. Recent studies have shown that both transcellular and paracellular mechanisms are key in nanoparticle entry into lymphatic vessels.[6−8] Research from our group has shown that the specific transport mechanisms used by lymphatic endothelial cells are dependent on nanoparticle size, shape, and surface chemistry, specifically PEG density.[8] We found that coating 100 nm nanoparticles with hydrophilic, neutrally charged poly(ethylene glycol) (PEG) leads to nanoparticle transport via both micropinocytosis and paracellular transport. Using computational models to study the kinetics behind these findings can aid in our understanding of how nanoparticle surface chemistry affects transcellular processes.[9−15] It is also well-established that the nanoparticle size influences the uptake mechanism; nanoparticles under 250 nm in diameter are typically taken up via micropinocytosis, while nanoparticles over 500 nm are preferentially taken up via macropinocytosis.[16] Indeed, features like shape, charge, and porosity contribute to transport mechanisms in endothelial cells, which have been explored.[17] Experiments examining rods of varying lengths and aspect ratios demonstrated that both design criteria affected uptake efficiency as well as uptake mechanism in HeLa and HUVEC cell lines.[18] Other groups also examined how the nanoparticle shape affects the uptake of rod-shaped nanoparticles in macrophages and the mechanisms driving uptake. They found that clathrin- and caveolin-mediated endocytosis drove the uptake of 100 nm rod-shaped nanoparticles.[19] Studies from Dasgupta et al. and Xu et al. observed similar results where cellular mechanisms drove the transport of rod-shaped nanoparticles into cells.[20,21] Charge is also a key contributor, and experiments have demonstrated that coating otherwise identical lipid nanoparticles with different charged coatings alters uptake and uptake mechanisms.[22] Here, we sought to model the kinetics of nanoparticle transport across lymphatic vessels. In this paper, we derive the equations and rate coefficients describing transport kinetics of nanoparticles, taking into account both transcellular and paracellular mechanisms. Additionally, we use transport data collected experimentally and simplify eqs 1−3 into a three-part problem of endocytosis, exocytosis, and paracellular transport, with the assumption that transport is driven in the direction of the concentration gradient from the interstitial tissue into the lumen of the vessel (Figure 1B, eqs 4−6). The resulting mathematical and computational framework can be used to extrapolate transport kinetics across similar cell layer problems and could be integrated with more complex machine learning-based techniques, like artificial neural networks, to predict the contribution of different transport mechanisms.

$$\frac{\partial C_1}{\partial t} = -\,(k_1 + k_3)C_1 + k_2C_2 \tag{4}$$

$$\frac{\partial C_2}{\partial t} = -\,(k_2 + k_4)C_2 + k_1C_1 \tag{5}$$

$$\frac{\partial C_3}{\partial t} = k_3C_1 + k_4C_2 \tag{6}$$

■ METHODS

Nanoparticle Formulation. Fluorescent carboxyl (COOH)-modified polystyrene (PS) nanoparticles (Thermo Fisher Scientific) were covalently modified with 5 kDa MW methoxy-PEG-amine (NH_2) (Creative PEGworks), as previously described.[23] Nanoparticles with different PEG conformations were generated using previously described methods.[24] Briefly, PS-COOH particles were suspended at 0.1% w/v in 200 mM borate buffer (pH = 8.2). PEG was conjugated to nanoparticles using 7 mM *N*-hydroxysulfosuccinimide (NHS) (Sigma) and 0.02 mM 1-Ethyl-3-(3-(dimethylamino)propyl) carbodiimide (EDC) (Invitrogen). The reaction was performed on a rotary incubator at room temperature for at least 4 h. Nanoparticles were collected using 100k MWCO centrifugal filters (Amicon Ultra; Millipore) and washed with deionized (DI) water to remove unconjugated PEG and other reactants. Nanoparticles were resuspended at 1% w/v in DI water and stored at 4 °C.

Nanoparticle Characterization. Dynamic light scattering (DLS) was used to measure the number-average hydrodynamic diameter and polydispersity index (PDI) of nanoparticles (NanoBrook Omni). Phase analysis light scattering (PALS) was used for measuring ζ-potential (NanoBrook Omni). Measurements were performed using a scattering angle of 90° at 25 °C. Measurements were based on the intensity of reflected light from scattered particles. Measurements were taken in 0.1× phosphate-buffered saline (PBS).

PEG Density Characterization. PEG density was determined using a previously published method.[24,25] Briefly, 5 kDa PEG-NH2 (Creative PEGworks) conjugated to fluorescein isothiocyanate (FITC) was conjugated to fluorescent (AlexaFluor555) 100 nm carboxyl-modified nanoparticles (Creative PEGworks). Using FITC-PEG-NH_2 standards, PEG grafting distance (D) and PEG density were estimated using the Flory radius of PEG (R_f) based on fluorescence intensity. The Flory radius of a polymer chain is defined as $R_f \sim \alpha N^{3/5}$, where N is the degree of polymerization and α is the effective monomer length. An unconstrained 5 kDa PEG chain has an R_f of 5.4 nm and occupies 22.7 nm^2. PEG density and conformation can be correlated to the ratio of R_f/D, with $R_f/D < 1$−1.5 yielding a mushroom conformation, 1−1.5< $R_f/D > 4$ yielding a brush conformation, and $R_f/D > 4$ yielding a dense brush conformation.

Nanoparticle Transport. LEC permeability was assessed using an established in vitro model that recapitulates in vivo lymphatic transport.[26] Briefly, primary human LECs (hLECs, Promocell C-12217) were seeded on 1.0 μm pore size and 12 mm transwell inserts (Falcon) at 200,000 cells/cm^2 and cultured in EGM2 (PromoCell) at 37 °C and 5% CO_2 for 48 h. Cells were pretreated with 1 μm/s transmural flow to simulate the interstitial fluid flow experienced in the tissue microenvironment. hLECs were treated with 10 μg/mL nanoparticles in the top compartment, and both the top and bottom compartments were sampled hourly until 12 h and also at 24 h. Fluorescence intensity was measured using a plate reader (Tecan), and nanoparticles transported were calculated using a standard curve. Transport experiments were performed in EGM2 without growth factors to avoid confounding effects of growth factors on transport mechanisms. To probe the transport mechanism, the following transport inhibitors were used: 100 nM Adrenomedullin (Abcam ab276417), 62.5 μM Dynasore (Sigma D7693), 62.5 μM Amiloride (Sigma A7410), or 10 μg/mL Brefeldin Alpha (BFA). Transport inhibitors were applied 2 h prior to introduction of nanoparticles. LEC monolayer integrity was confirmed after experiments using immunofluorescence.

For simulated cigarette smoke exposure, cigarette smoke extract (CSE) was prepared as previously described and added to EGM2 without growth factors to avoid confounding effects of growth factors on transport mechanisms at a final concentration of 2% v/v. Cells were pretreated with 1 μm/s transmural flow to simulate the interstitial fluid flow experienced in the tissue microenvironment 16 h before experimentation. hLECs were treated with 10 μg/mL nanoparticles in the top compartment, and both the top and bottom compartments were sampled hourly for 12 h, and also, at 24 h, CSE was applied 2 h prior to the introduction of nanoparticles.

Computational Model Solving. Eqs 1−3 were generated to model the three-compartment model of nanoparticle transport across LECs (Figure 1A). The following assumptions were made to simplify the model: (1) transport between cells is unidirectional along the concentration gradient since $[C_1] \gg [C_3]$ $(k_4 = 0)$ and (2) reuptake of nanoparticles from compartment C_3 to C_2 is negligible (k_7, k_8 = 0). Under these assumptions, eqs 1−3 become eqs 4−6 (Figure 1B).

Experimental data of C_1 and C_3 were used to extrapolate C_2, assuming that nanoparticle mass and fluorescence were conserved. These data were normalized to $C = C/C_{\text{total}}$. The normalized concentration over time data was used to estimate k parameters using the MatLab "lsqcurvefit" function. Levenberg−Marquardt, or the damped least-squares method, was used to solve the nonlinear least-squares optimization problem (eq 7):

$$\min_x \left| |F(x, x\text{data}) - y\text{data}\|_2^2 \right. = \min_x \sum_i (F(x, x\text{data}_i) - (y\text{data}_i))^2 \qquad (7)$$

For parameter estimation, k values were constrained to be positive to match the kinetics outlined in eqs 4−6 and Figure 1B.

Statistics. Group analysis was performed using a two-way ANOVA, followed by Tukey's post-test. Unpaired Student's t test was used to examine differences between only two groups. A value of $p < 0.05$ was considered significant (GraphPad). All data are presented as mean ± standard error of the mean (SEM) and representative of at least two repeat experiments.

■ RESULTS

Transport Efficiency of Nanoparticles across LECs Can Be Fitted to a Three-Compartment Kinetic Model.

To be able to fully model the transport kinetics within the three compartments (Figure 2A), C_1 (top compartment, interstitial tissue where nanoparticles are injected), C_2 (intracellular), and C_3 (bottom compartment, vessel lumen that leads to the lymph nodes), we first collected data on concentration change over time within C_1 and C_3 (Figure 2B). We formulated 40−150 nm PEGylated nanoparticles[23,24] from unmodified 103 ± 5 and 40 ± 2 nm. 100 and 40 nm nanoparticles were selected for this study as they lie within the 10−250 nm size range reported to enter lymphatic vessels and transport to lymph nodes.[8,27−29] Addition of PEG increased

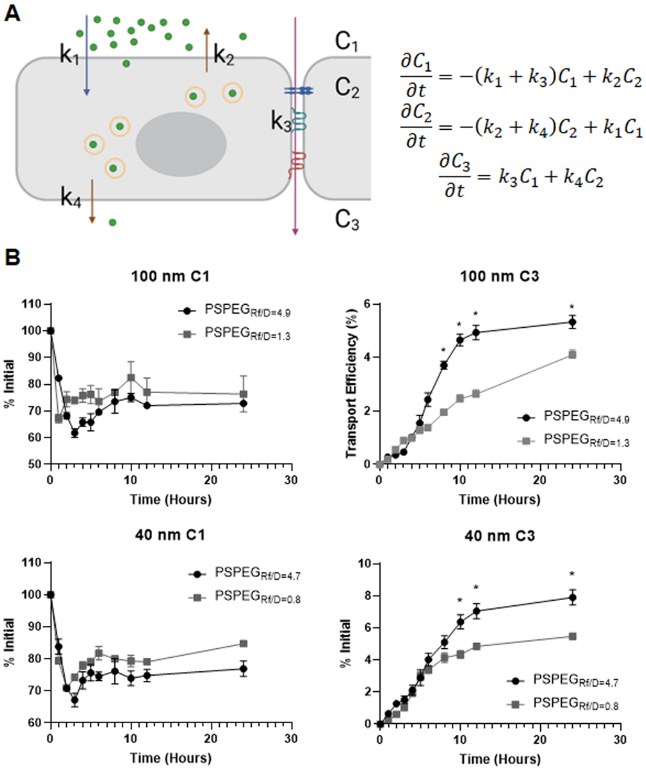

Figure 2. PEG coating improves transport of 100 and 40 nm NP across LECs. (A) Schematic of the transport model and associated differential equations. (B) Top: Percent of 100 nm fully PEGylated (PSPEG$_{Rf/D=4.9}$) and partially PEGylated NP (PSPEG$_{Rf/D=1.3}$) in the top compartment and transported across LEC monolayer into the bottom compartment over time. Bottom: Percent of 40 nm NP fully PEGylated (PSPEG$_{Rf/D=4.7}$) and partially PEGylated NP (PSPEG$_{Rf/D=0.8}$) in the top compartment and transported across LEC monolayer into the bottom compartment over time. Data presented as mean ± SEM (*$p < 0.05$), n = 4 samples and n > 2 repeat experiments.

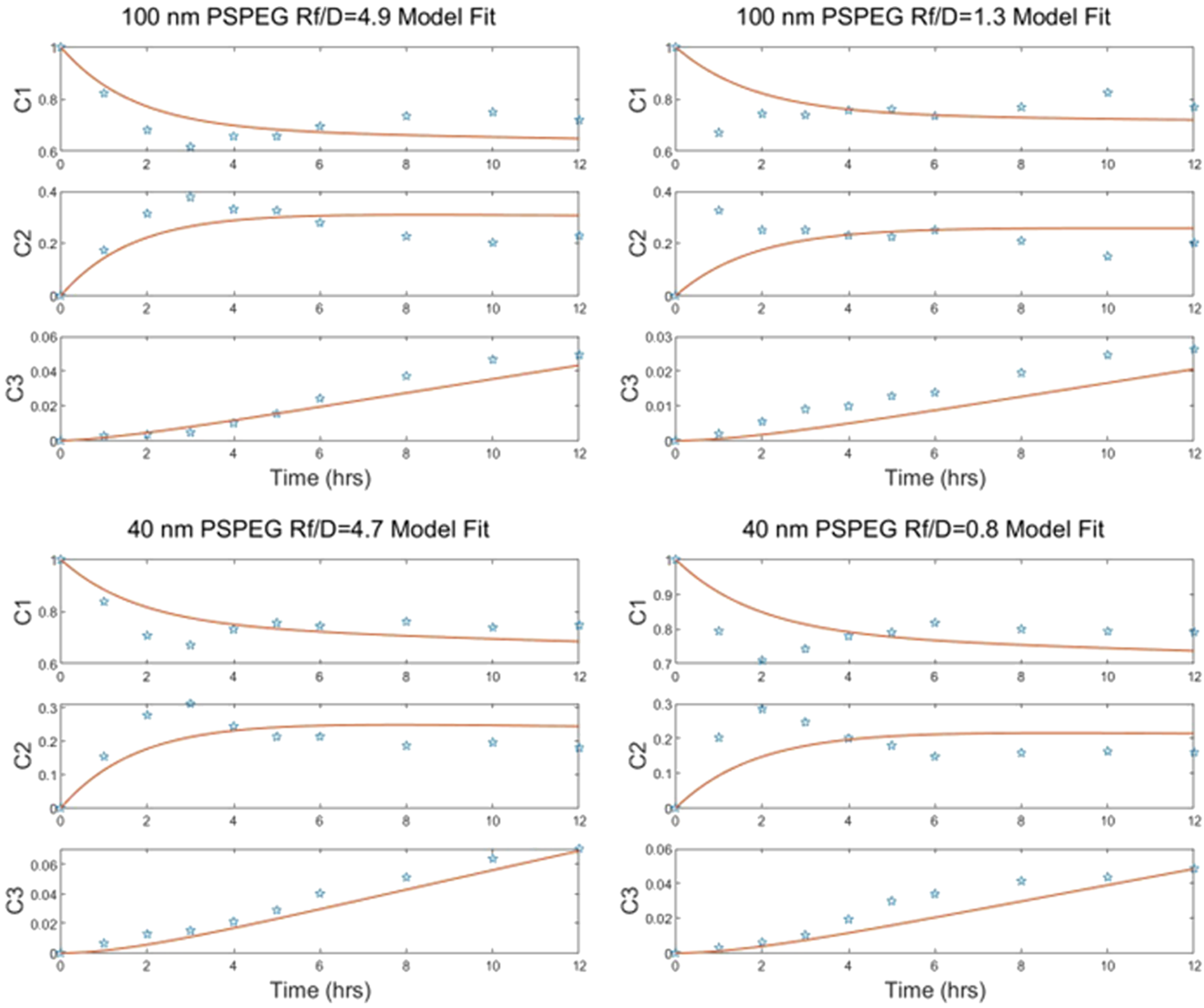

Figure 3. Nanoparticle transport across LECs can be modeled with our three-compartment kinetic model. Normalized experimental concentration data (stars) fitted against the system of differential equations (solid line).

Table 1. Calculated k Values of the System of Differential Equations Describing Nanoparticle Transport across LECs for Different Nanoparticle Formulations

rate constants (μg mL^{-1} h^{-1})	100 nm PSPEG$_{Rf/D=4.9}$	100 nm PSPEG$_{Rf/D=1.3}$	40 nm PSPEG$_{Rf/D=4.7}$	40 nm PSPEG$_{Rf/D=0.8}$
k_1	1.9	1.5	1.5	1.2
k_2	3.9	3.5	4.0	3.2
k_3	0.013	0.012	0.014	0.011
k_4	0.13	0.074	0.26	0.21

nanoparticle hydrodynamic diameter to 122 ± 6 nm (partial PEG) and 142 ± 3 nm (dense PEG) and 43 ± 2 nm (partial PEG) and 49 ± 3 nm (dense PEG) (Figure S1A). PEGylated nanoparticles also displayed a near-neutral ζ − potential (Figure S1B). Using these nanoparticles, we found that C_1 was reduced to 60−70% of the initial nanoparticle concentration placed in the top well, after which C_1 increased again when nanoparticles were exocytosed into the top compartment (Figure 2B). We confirmed that this phenomenon was due to exocytosis by employing Brefeldin A, an exocytosis inhibitor, in our transport model, where we observed that exocytosis back into C_1 was reduced compared to untreated wells (Figure 2). We also confirmed that densely PEGylated nanoparticles were transported the most efficiently compared to partially PEGylated nanoparticles, with 5.3 ± 0.2% nanoparticles transported into C_3 for densely PEGylated 100 nm nanoparticles, compared to 4.1 ± 0.2% for partially PEGylated nanoparticles (Figure 2B). Similarly, 40 nm densely PEGylated nanoparticles had 7.9 ± 0.5% of nanoparticles transported into C_3, compared to 5.5 ± 0.2% for the partially PEGylated nanoparticles (Figure 2B).

We then used C_1 and C_3 data (Figure 2B) and a nonlinear, least-squares, curve fitting algorithm (Figure 3) to estimate the kinetics (k) parameters in the system of differential equations (Table 1). Based on these k values, we can see that the initial uptake and release of nanoparticles at the top compartment interface (k_1 and k_2) is the dominant reaction, indicated by the order of magnitude difference compared to k_3 and k_4. Another

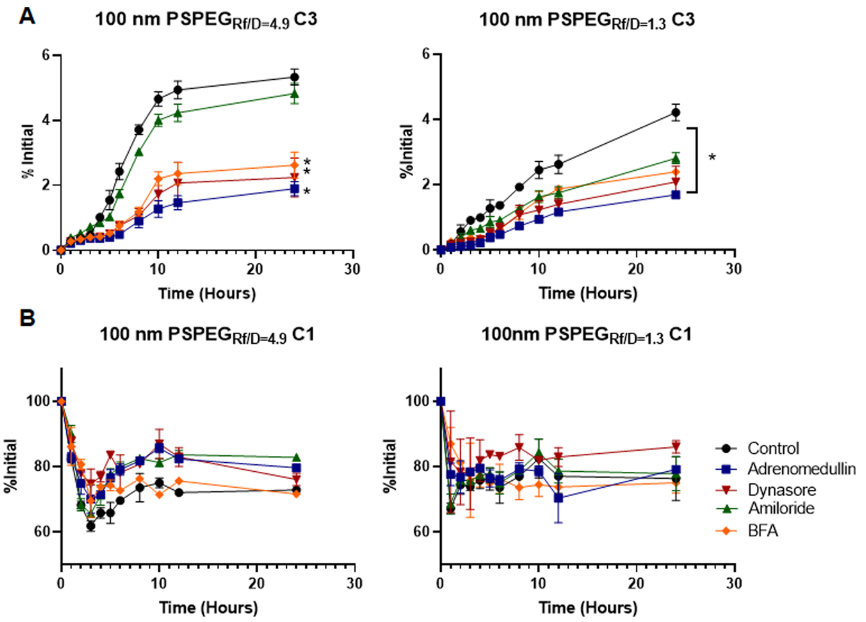

Figure 4. Kinetic model captures transport mechanisms governing NP transport across LECs. Percent transport of 100 nm fully PEGylated (PSPEG$_{Rf/D=4.9}$) and partially PEGylated NP (PSPEG$_{Rf/D=1.3}$) in the (A) bottom (C_3) and (B) top (C_1) compartments in the presence of transport inhibitors. Data presented as mean ± SEM (*$p < 0.05$) $n = 2–4$.

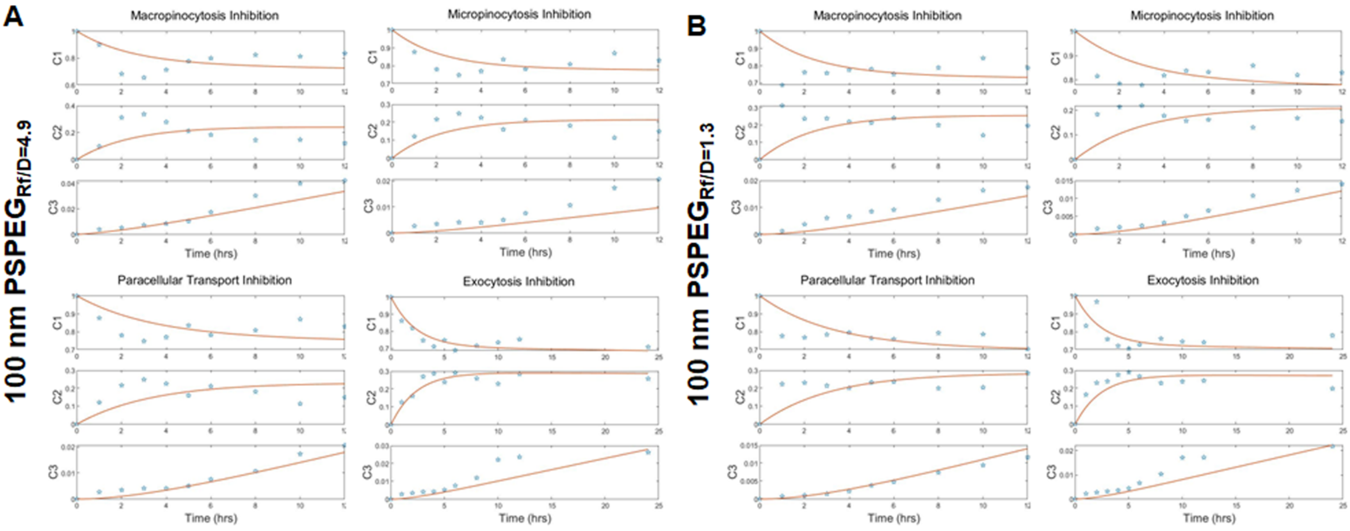

Figure 5. Kinetic model captures transport mechanisms governing NP transport across LECs. Percent transport of 100 nm fully PEGylated (PSPEG$_{Rf/D=4.9}$) and partially PEGylated NP (PSPEG$_{Rf/D=1.3}$) in the presence of transport inhibitors. Normalized experimental concentration data (stars) fitted against the system of differential equations (solid line) including different transport inhibitors. (A) Fully PEGylated 100 nm $R_f/D = 4.9$ nanoparticles and (B) partially PEGylated $R_f/D = 1.3$ nanoparticles.

trend to note is that k_3, describing paracellular transport, is the smallest parameter. This indicates that cellular mechanisms, including endocytosis and micropinocytosis, are driving nanoparticle transport across LEC barriers. Importantly, transport trends with respect to formulation are captured within the model. k_4, a key parameter for measuring the transport of nanoparticles into the simulated vessel, increases from 0.13 μg mL^{-1} h^{-1} for the larger 100 nm PSPEG$_{Rf/D=4.9}$ nanoparticles to 0.26 μg mL^{-1} h^{-1} for the smaller 40 nm PSPEG$_{Rf/D=4.7}$ nanoparticles.

Size and Surface Chemistry of Nanoparticles Affect Their Transport via Macropinocytosis across LECs. Next, we investigated how the kinetics changed for different cellular transport mechanisms. Again, we used partially and densely PEGylated, 40–150 nm nanoparticles. As in our prior study, we found that 100 nm densely PEGylated nanoparticles were not transported by macropinocytosis and that both paracellular and transcellular transport were involved, indicated by reduced transport upon introduction of transport inhibitors (Figure 4A). Interestingly, for partially PEGylated nanoparticles, all transport mechanisms were involved in nanoparticle accumulation in C_3 (Figure 4A). The introduction of transport inhibitors generally reduced the depletion of nanoparticles from C_1: for both 100 nm PSPEG$_{Rf/D=4.9}$ and PSPEG$_{Rf/D=1.3}$, inhibiting micropinocytosis reduced this phenomenon the greatest, albeit not significantly different (Figure 4B). These transport data including transport inhibitors were then incorporated into our three-compartment kinetic model and

Table 2. Calculated k Values of the System of Differential Equations Describing Transport of 100 nm $\mathrm{PSPEG}_{Rf/D=4.9}$ across LECs in the Presence of Different Transport Inhibitors

rate constants (μg mL^{-1} h^{-1})	100 nm $\mathrm{PSPEG}_{Rf/D=4.9}$	+amiloride	+dynasore	+adrenomedullin	+BFA
k_1	1.9	1.2	1.0	1.70	1.6
k_2	3.9	3.0	3.6	2.2	1.6
k_3	0.013	0.02	0.2	0.005	0.019
k_4	0.13	0.10	0.041	0.088	0.032

Table 3. Calculated k Values of the System of Differential Equations Describing Transport of 100 nm $\mathrm{PSPEG}_{Rf/D=1.3}$ across LECs in the Presence of Different Transport Inhibitors

rate constants (μg mL^{-1} h^{-1})	100 nm $\mathrm{PSPEG}_{Rf/D=1.3}$	+amiloride	+dynasore	+adrenomedullin	+BFA
k_1	1.5	1.0	0.7	1.90	1.3
k_2	3.5	2.8	2.6	2.2	1.2
k_3	0.012	0.01	0.18	0.002	0.020
k_4	0.074	0.10	0.057	0.055	0.026

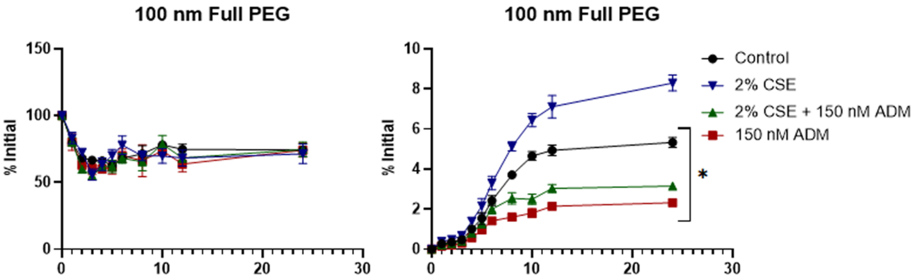

Figure 6. Cigarette smoke extract increases lymphatic permeability to nanoparticles. Percent transport of 100 nm fully PEGylated ($\mathrm{PSPEG}_{Rf/D=4.9}$) and partially PEGylated NP ($\mathrm{PSPEG}_{Rf/D=1.3}$) in the (A) bottom ($C_3$) and (B) top ($C_1$) compartments in the presence of CSE and transport inhibitors. Data presented as mean ± SEM ($^*p < 0.05$) from $n > 2$ repeat experiments and $n = 4+$ replicates.

fitted to the system of differential equations using a nonlinear, least-squares, curve fitting algorithm, resulting in curve fitting (Figure 4C,D). We used our computational model to curve-fit solutions and extrapolate transport coefficients (Figure 5). Solved parameters k for equations with respect to nanoparticle formulation are found in Tables 2 and 3. From these k values, we can see trends in the presence of inhibitors similar to the control transport experiments: For both densely and partially PEGylated nanoparticles, k_1 and k_2 (uptake and rerelease of nanoparticles into C_1) are larger than k_3 and k_4 (transcellular and paracellular transport of nanoparticles into C_3). To further probe this phenomenon, we introduced BFA, which prevents the processing of endosomes via the Golgi apparatus and thus prevents exocytosis. With BFA treatment, we see a reduction in transport efficiency compared to the vehicle control. Furthermore, we see a trend where nanoparticles are not emitted back into C_1 (uptake interface) as quickly as other treatments (not significant).

Our computational model captures how the inclusion of transport inhibitors affects mechanisms used for transport. Removing paracellular transport resulted in an increase in k_1 for partially PEGylated nanoparticles. When micropinocytosis was inhibited, k_1 dropped from 1.9 to 1.0 and 1.5 to 0.7 μg mL^{-1} h^{-1} for densely and partially PEGylated 100 nm nanoparticles, respectively. k_3, which represents paracellular transport, in contrast, increased nearly 10-fold, suggesting that an increased concentration gradient drives more nanoparticles across LECs via paracellular transport. When exocytosis was inhibited at both interfaces, we see that k_2 and k_4 are at a minimum relative to other treatments, indicating that the model captures this prevention of exocytosis at both interfaces. Even though our experimental data suggest that inhibition of macropinocytosis does not significantly modulate densely PEGylated 100 nm nanoparticle transport across LECs, our computational data show a reduction in k_1 upon treatment with amiloride from 1.9 to 1.2, suggestive of the complex relationship between the regulation of transcellular transport mechanisms in biological systems.

Introduction of Cigarette Smoke Extract to the Model Increases Lymphatic Permeability to Nanoparticles. Previous studies have demonstrated that the presence of cigarette smoke can increase the permeability of LECs to model protein and dextrans and that the junctions between LECs become discontinuous and dysregulated.[30] Here, we sought to see how lymphatic permeability to our model nanoparticle changed in the presence of cigarette smoke extract (CSE). We found that in the presence of CSE, the transport of nanoparticles across lymphatics increased almost 2-fold from 5.3 ± 0.2 to 8.3 ± 0.4% (Figure 6). Since previous studies have suggested that this could be due to increased paracellular transport, we inhibited this mechanism using adrenomedullin. We found that inhibiting paracellular transport in the presence of CSE caused a significant decrease in transport. This transport was still slightly higher than when paracellular transport was inhibited in the normal system. These transport trends were also captured by our computational model, where k_3 modeling paracellular transport rose from 0.013 to 0.032 μg/mL h in the presence of CSE and dropped to 0.001 μg/mL h when paracellular transport was inhibited (Table 4).

Table 4. Calculated k Values of the System of Differential Equations Describing Transport of 100 nm PSPEG$_{Rf/D=4.9}$ across LECs in the Presence of Cigarette Smoke Extract

rate constants (μg mL^{-1} h^{-1})	vehicle control	2% CSE	2% CSE + ADM	ADM
k_1	1.44	1.34	1.76	1.70
k_2	3.7	2.8	3.2	2.1
k_3	0.013	0.032	0.005	0.002
k_4	1.24	1.78	0.98	0.045

■ DISCUSSION

In this study, we probed how nanoparticle formulation parameters, including size and surface chemistry, influenced both the transport efficiency and transport mechanism into lymphatic vessels. We found that increasing the density of PEG on the surface of nanoparticles improved transport efficiency, with maximal transport efficiency occurring with the smaller, 40 nm densely PEGylated nanoparticles. We also observed that nanoparticle transport mechanism is dependent on formulation, notably that macropinocytosis does not drive transport for 100 nm densely PEGylated nanoparticles. Using these experimental results, we fitted our data into a set of differential equations describing the three-compartment problem including endocytosis, exocytosis, and paracellular transport. This computational framework produced parameters to describe transport kinetics and allow for the quantitative analysis of the driving mechanisms of transport and formulation parameters.

Lymphatic vessels exist throughout the entire body and are known for transporting cells, fluid, and particulates from peripheral tissues to the local draining lymph nodes, where the adaptive immune response is formed. Lymphatics are important drug delivery targets as they transport immune modulatory therapies to the lymph nodes, and this can improve vaccine and immunotherapeutic efficacy.[31] A study from Triacca et al. provided evidence that LECs are a barrier to delivery into lymphatic vessels.[26] They demonstrated that when micropinocytosis was inhibited with Dynasore, the transport efficiency of albumin and dextran across the LECs decreased significantly—a clear indication that LECs serve as barriers. We also recently demonstrated first insights into the transport mechanisms involved in the transport of nanoparticles across lymphatic barriers. We found that both paracellular and transcellular transport mechanisms were key in crossing lymphatic barriers, with LECs relying on clathrin-mediated endocytosis to mediate transport of PEGylated nanoparticles.[24] Here, we demonstrate that the key drivers of nanoparticle transport across LECs are uptake and exocytosis along with paracellular transport.

Our prior studies demonstrated that macropinocytosis is affected by size and surface chemistry and that endocytosis and exocytosis mechanisms are crucial for nanoparticle transport across LECs. We have confirmed this here and extrapolated the transport coefficients for these systems, which further confirm the importance of more than one mechanism of transport. Researchers have also demonstrated that macro- and micropinocytosis are involved in nanoparticle transport across endothelial cells in tumors and the blood−brain barrier.[32−38] Rabanel et al. demonstrated that nanoparticles coated with 5 kDa PEG were taken up primarily via macropinocytosis pathways in brain endothelial cells.[39] Tehrani et al. found that inhibiting micropinocytosis reduced transcytosis across brain endothelial cells by 60% for 5 kDa PEG-coated nanoparticles, while transcytosis of 2 kDa PEG-coated nanoparticles was reduced only by 25% after inhibiting micropinocytosis.[40] These findings suggest that endocytosis drives nanoparticle uptake and that transcytosis pathways may differ with nanoparticle size and different amounts and density of PEG, corroborating the results in this study. Additionally, studies have demonstrated that nanoparticle transport across brain microvascular endothelium can be enhanced by taking advantage of the existing receptor-mediated transcytosis, such as that of albumin (clathrin/caveolin-dependent).[36,41−44] Collectively, these studies indicate that endothelial barriers serve as a barrier to drug delivery and that nanoparticle uptake is a key step in overcoming these barriers. Our studies also demonstrate the importance of exocytosis mechanisms in mediating nanoparticle transport across cellular barriers; how nanoparticles and other materials are trafficked within cells before being exocytosed into lumen, or back into interstitial spaces, needs further exploration. A key aspect of this has been shown to be the polarization of cells, tissues, and subsequent transport proteins. This subject has been thoroughly reviewed,[17] and studies have indicated that the presence of key proteins, including PAR6, PAR3, PKC-3 (aPKC), CDC42, and Rab5, are key in endosomal trafficking in a polarity-dependent manner. Ablation or combinations of these proteins results in dysregulated transport and tissue organization.[45−48] Similar polarization proteins likely play a key role in the transport of nanoparticles into and across LECs, and trafficking of nanoparticles within LECs, but precise mechanisms are unknown.

Our data also demonstrate that nanoparticle transport kinetics are affected during disease. We showed that upon treatment with CSE, there was an increase in paracellular transport as well as exocytosis out of the cell into the "vessel lumen" compartment, while reducing micropinocytosis and exocytosis into the interstitial space compartment. These data corroborate our prior findings that CSE increases lymphatic permeability in vitro and in vivo and leads to aberrant junction morphology.[49] Researchers have also shown that a host of other diseases such as lymphedema, inflammatory bowel disease, and viral infections can affect the permeability of lymphatic vessels in vivo by modulating their junctions.[50−58] For instance, after vaccinia infection in the skin, lymphatic capillaries exhibit "zippering," meaning that their normally discontinuous cell−cell junctions become continuous after infection.[55] However, the kinetics and specific transport mechanisms that are affected in diseases still remain mostly poorly understood and we here present a novel method for studying transport kinetics across LECs.

Computational methods and frameworks to model drug delivery into tissues and across endothelial barriers have been used to study the regulation of nanoparticle transport and to guide nanoparticle design to target tissues of interest. One of the key considerations when applying a computational model to physiological phenomena is deciding what type of model to employ. In our study, we generated a three-compartment model of the lymphatic endothelium and used the Levenberg−Marquardt algorithm for parameter estimation to solve our nonlinear least-squares parameter optimization problem for our system of ODEs. This algorithm was used as it is more robust than the more common Gauss−Newton algorithm, especially when the data are not well-behaved or the starting parameters are far from the solution parameters, as is often the case when modeling physiological data.[59]

In addition to computational modeling of drug delivery on the larger tissue level, studies have also sought to model drug and nanoparticle transport across, and interactions with, cells and cell layers. Chou et al. developed a pharmacokinetic model to examine gold nanoparticle kinetics in rat models. Through the development of their model, they examined how size affected kinetics.[60] Interestingly, based on their physiological data, they were able to modify a classical pharmacokinetic modeling framework to hypothesize nanoparticle-specific pathways and kinetics with respect to size. While their model focused on the uptake and clearance of nanoparticles at the organ scale, the formation of their model indicated that classical approaches employed for small molecule pharmacokinetic modeling did not translate to nanoparticle modeling and that administration route-specific data and modeling is needed to improve approaches to modeling nanoparticle pharmacokinetics. A key consideration from their study is that the lymphatics and lymph nodes were not included in their model, highlighting the gap in knowledge regarding nanoparticle pharmacokinetics in these key tissues. Using multicompartment models to examine nanoparticle transport across endothelial layers is an interesting area of research, especially when targeting tumors. Two recent studies used similar models to examine nanoparticle accumulation in tissues and tumors of interest. Both studies were able to demonstrate that multicompartment models and systems of differential equations were able to recapitulate in vivo data. More so in their studies, they highlighted the predictive power of these models by predicting how nanoparticle formulation parameters could alter transport efficiency.[61,62] A key part of these studies is linking theoretical kinetic data with in vivo data. Neubauer et al. were able to use MRI as a method to validate three-compartment models in pharmacological studies. In this study, they were able to observe in vivo and in real time the binding of perfluorocarbon nanoparticles with $\alpha_v\beta_3$-integrins involved in atherosclerosis.[63] While these studies highlight the utility of multicompartment pharmacokinetic modeling, focus has primarily been on models at the system and tissue scale, with a lack of focus on precise cellular mechanisms regulating transport. Furthermore, most multicompartment kinetic models focus on small molecule drugs and there is a growing need to apply these modeling strategies for nanoparticles, as they are becoming more prevalent in the clinic. A recent paper from Khan et al. employed a similar transwell-based model as outlined in our study.[15] They generated a three-compartment model and fitted observed transport data to a system of kinematic equations to solve for the transport coefficients governing their model. This study highlighted how artificial neural networks (ANNs) can be used as a method to statistically model and solve kinematic transport equations similar to the ones set forth in our study. In their model, they observed a steady accumulation of nanoparticles within the intracellular compartment, in contrast to the rapid uptake and release observed in our model. Collectively, these studies demonstrate the utility of computational models and how they can be employed to better understand how the transport of key agents in tissues of interest is regulated. Our work builds on these concepts by using computational methods to examine what mechanisms are driving transport as well as using these methods to quantitatively describe how formulation parameters can affect transport efficiency.

One of the interesting findings from our study is the nanoparticle uptake and release back into the top well. This was reduced when we inhibited exocytosis mechanisms, suggesting that exocytosis plays a key role in nanoparticle transport. This phenomenon has been observed in other studies, including one by Georgieva et al., which showed how caveolin-mediated uptake of nanoparticles by endothelial cells peaked at 30 min before being released back into the environment.[64] This relatively rapid uptake and release of nanoparticles is similar to what occurred in our study, reinforcing that endocytosis pathways are key when examining nanoparticle transport. Another study from Fiorentino et al. observed a similar phenomenon where 20−100 nm PS nanoparticles were rapidly taken up by blood outgrowth endothelial cells and released back into cell culture within 4 h. Furthermore, they observed that nanoparticles localized with caveolin and that inhibiting endocytotic pathways with chemical inhibitors, including Dynasore, prevented nanoparticle uptake.[65] This endocytosis-mediated uptake and translocation of nanoparticles is similarly observed in our study, with the administration of the micropinocytosis inhibitor Dynasore decreasing the rapid uptake of nanoparticles seen in untreated controls. Rapid uptake and release of nanoparticles has been observed in a variety of cell types, including epithelial cells, fibroblasts, and macrophages.[66−69]

■ CONCLUSIONS

In summary, our study demonstrates that a dense coating of PEG ($R_f/D > 4$) is required to maximize transport across lymphatic barriers. These findings are consistent with prior work demonstrating that PEG enhances uptake and transport across other endothelial barriers as well as the cellular mechanisms involved in this transport. This work is one of the first to closely examine the kinetics of nanoparticle transport across the lymphatic barrier. Our computational framework can be integrated with more complex machine learning-based techniques, such as artificial neural networks, to predict the contributions of different transport mechanisms and drive formulation strategies for nanoparticles that will maximize transport across lymphatics and to the LNs, which is crucial for future development of immune modulatory therapeutic strategies.

■ ASSOCIATED CONTENT

Supporting Information

The Supporting Information is available free of charge at https://pubs.acs.org/doi/10.1021/acs.molpharmaceut.3c00720.

Formulation of 100 and 40 nm PEGylated nanoparticles (PDF)

■ AUTHOR INFORMATION

Corresponding Author

Katharina Maisel − *Department of Bioengineering, University of Maryland College Park, College Park, Maryland 20742, United States;* orcid.org/0000-0002-3560-9751; Email: maiselka@umd.edu

Authors

Jacob McCright − *Department of Bioengineering, University of Maryland College Park, College Park, Maryland 20742, United States*

Jenny Yarmovsky − *Department of Bioengineering, University of Maryland College Park, College Park, Maryland 20742, United States*

Complete contact information is available at:
https://pubs.acs.org/10.1021/acs.molpharmaceut.3c00720

Notes

The authors declare no competing financial interest.

ACKNOWLEDGMENTS

We would like to thank the UMD Bioworkshop core facility and Michele Kaluzienski for manuscript editing. This work was funded by NIH MIRA R35 (K.M.), NSF CAREER Award (K.M.), the AHA Predoctoral Research Fellowship (J.M.), and Clark midcareer doctoral fellowship (J.M.).

ABBREVIATIONS

PEG, poly(ethylene glycol); PS, polystyrene; DLS, dynamic light scattering; PDI, polydispersity index; PALS, phase analysis light scattering; R_f, Flory radius; *D*, grafting distance; LECs, lymphatic endothelial cells; ODE, ordinary differential equation; NHS, *N*-hydroxysulfosuccinimide; EDC, 1-ethyl-3-(3-(dimethylamino)propyl) carbodiimide; ANNs, artificial neural networks

REFERENCES

(1) Mdzinarashvili, T.; Khvedelidze, M.; Partskhaladze, T.; Nafee, N.; Lehr, C.-M.; Schneider, M. Stability of drug delivery PLGA nanoparticles: Calorimertric approach. *Drug Deliv.* **2011**, 189−205.

(2) Mudshinge, S. R.; Deore, A. B.; Patil, S.; Bhalgat, C. M.; et al. Nanoparticles: Emerging carriers for drug delivery. *Saudi Pharm. J.* **2011**, *19* (3), 129−141.

(3) Friedman, A. D.; Claypool, S. E.; Liu, R. The smart targeting of nanoparticles. *Curr. Pharm. Des.* **2013**, *19* (35), 6315−6329.

(4) Kamaly, N.; et al. Degradable Controlled-Release Polymers and Polymeric Nanoparticles: Mechanisms of Controlling Drug Release. *Chem. Rev.* **2016**, *116* (4), 2602−2663.

(5) Ghaffarian, R.; Muro, S. Models and methods to evaluate transport of drug delivery systems across cellular barriers. *J. Vis. Exp.* **2013**, *80*, No. e50638.

(6) Triacca, V.; et al. Transcellular Pathways in Lymphatic Endothelial Cells Regulate Changes in Solute Transport by Fluid Stress. *Circ. Res.* **2017**, *120* (9), 1440−1452.

(7) Srinivasan, S.; Vannberg, F. O.; Dixon, J. B. Lymphatic transport of exosomes as a rapid route of information dissemination to the lymph node. *Sci. Rep.* **2016**, *6* (1), 24436.

(8) McCright, J.; et al. Nanoparticles with dense poly(ethylene glycol) coatings with near neutral charge are maximally transported across lymphatics and to the lymph nodes. *Acta Biomater.* **2022**, *145*, 146−158.

(9) Tian, F.; et al. Computer simulation studies on the interactions between nanoparticles and cell membrane. *Sci. China Chem.* **2014**, *57* (12), 1662−1671.

(10) Lin, X.; Li, Y.; Ning, G. Nanoparticle's Size Effect on Its Translocation Across a Lipid Bilayer: A Molecular Dynamics Simulation. *J. Comput. Theor. Nanosci.* **2010**, *7*, 269−276.

(11) Jayasinghe, M. K.; et al. The Role of in silico Research in Developing Nanoparticle-Based Therapeutics. *Front. Digit Health* **2022**, *4*, No. 838590.

(12) Liu, Y.; Shah, S.; Tan, J. Computational Modeling of Nanoparticle Targeted Drug Delivery. *Rev. Nanosci. Nanotechnol.* **2012**, *1*, 66−83.

(13) Ramezanpour, M.; et al. Computational and experimental approaches for investigating nanoparticle-based drug delivery systems. *Biochim. Biophys. Acta* **2016**, *1858* (7, Part B), 1688−1709.

(14) Groh, C. M.; et al. Mathematical and computational models of drug transport in tumours. *J. R. Soc. Interface* **2014**, *11* (94), No. 20131173.

(15) Khan, A. I.; et al. Quantification of kinetic rate constants for transcytosis of polymeric nanoparticle through blood-brain barrier. *Biochim. Biophys. Acta* **2018**, *1862* (12), 2779−2787.

(16) Pedrioli, G.; Paganetti, P. Hijacking Endocytosis and Autophagy in Extracellular Vesicle Communication: Where the Inside Meets the Outside. *Front. Cell Dev. Biol.* **2021**, *8*, No. 595515.

(17) Di Fiore, P. P.; von Zastrow, M. Endocytosis, signaling, and beyond. *Cold Spring Harb. Perspect. Biol.* **2014**, *6* (8), No. a016865, DOI: 10.1101/cshperspect.a016865.

(18) Liu, X.; et al. Size Dependent Cellular Uptake of Rod-like Bionanoparticles with Different Aspect Ratios. *Sci. Rep.* **2016**, *6* (1), 24567.

(19) Xie, X.; et al. The Effect of shape on Cellular Uptake of Gold Nanoparticles in the forms of Stars, Rods, and Triangles. *Sci. Rep.* **2017**, *7* (1), 3827.

(20) Xu, Z. P.; et al. Subcellular compartment targeting of layered double hydroxide nanoparticles. *J. Controlled Release* **2008**, *130* (1), 86−94.

(21) Dasgupta, S.; Auth, T.; Gompper, G. Shape and orientation matter for the cellular uptake of nonspherical particles. *Nano Lett.* **2014**, *14* (2), 687−693.

(22) Voigt, J.; Christensen, J.; Shastri, V. P. Differential uptake of nanoparticles by endothelial cells through polyelectrolytes with affinity for caveolae. *Proc. Natl. Acad. Sci. U. S. A.* **2014**, *111* (8), 2942−2947.

(23) Nance, E. A.; et al. A dense poly(ethylene glycol) coating improves penetration of large polymeric nanoparticles within brain tissue. *Sci. Transl. Med.* **2012**, *4* (149), 149ra119.

(24) McCright, J.; et al. Nanoparticles with dense poly(ethylene glycol) coatings with near neutral charge are maximally transported across lymphatics and to the lymph nodes. *Acta Biomater.* **2022**, *145*, 146.

(25) Kelley, W. J.; et al. PEGylation of model drug carriers enhances phagocytosis by primary human neutrophils. *Acta Biomater.* **2018**, *79*, 283−293.

(26) Triacca, V.; et al. Transcellular Pathways in Lymphatic Endothelial Cells Regulate Changes in Solute Transport by Fluid Stress. *Circ. Res.* **2017**, *120* (9), 1440−1452.

(27) McCright, J.; et al. Targeting Lymphatics for Nanoparticle Drug Delivery. *Front. Pharmacol.* **2022**, *13*, No. 887402.

(28) Reddy, S. T.; et al. Exploiting lymphatic transport and complement activation in nanoparticle vaccines. *Nat. Biotechnol.* **2007**, *25* (10), 1159−1164.

(29) Reddy, S. T.; et al. In vivo targeting of dendritic cells in lymph nodes with poly(propylene sulfide) nanoparticles. *J. Controlled Release* **2006**, *112* (1), 26−34.

(30) Summers, B. D.; et al. Lung lymphatic thrombosis and dysfunction caused by cigarette smoke exposure precedes emphysema in mice. *Sci. Rep.* **2022**, *12* (1), 5012.

(31) Maisel, K.; et al. Exploiting lymphatic vessels for immunomodulation: Rationale, opportunities, and challenges. *Adv. Drug Deliv. Rev.* **2017**, *114*, 43−59.

(32) Aguilera, G.; et al. Carboxymethyl cellulose coated magnetic nanoparticles transport across a human lung microvascular endothelial cell model of the blood−brain barrier. *Nanoscale Adv.* **2019**, *1* (2), 671−685.

(33) Ahn, S. I.; et al. Microengineered human blood−brain barrier platform for understanding nanoparticle transport mechanisms. *Nat. Commun.* **2020**, *11* (1), 175.

(34) Chattopadhyay, N.; et al. Solid lipid nanoparticles enhance the delivery of the HIV protease inhibitor, atazanavir, by a human brain endothelial cell line. *Pharm. Res.* **2008**, *25* (10), 2262−2271.

(35) Francia, V.; Aliyandi, A.; Salvati, A. Effect of the development of a cell barrier on nanoparticle uptake in endothelial cells. *Nanoscale* **2018**, *10* (35), 16645−16656.

(36) Kim, H. R.; et al. Low-density lipoprotein receptor-mediated endocytosis of PEGylated nanoparticles in rat brain endothelial cells. *Cell. Mol. Life Sci.* **2007**, *64* (3), 356−364.

(37) Moghimi, S. M.; Simberg, D. Nanoparticle transport pathways into tumors. *J. Nanopart. Res.* **2018**, *20* (6), 169.

(38) Skotland, T.; Sandvig, K. Transport of nanoparticles across the endothelial cell layer. *Nano Today* **2021**, *36*, No. 101029.

(39) Rabanel, J.-M.; et al. Transport of PEGylated-PLA nanoparticles across a blood brain barrier model, entry into neuronal cells and in vivo brain bioavailability. *J. Controlled Release* **2020**, *328*, 679−695.

(40) Tehrani, S. F.; et al. Length of surface PEG modulates nanocarrier transcytosis across brain vascular endothelial cells. *Nanomedicine* **2019**, *16*, 185−194.

(41) Kreuter, J. Mechanism of polymeric nanoparticle-based drug transport across the blood-brain barrier (BBB). *J. Microencapsul.* **2013**, *30* (1), 49−54.

(42) Wang, Z.; et al. Size and Dynamics of Caveolae Studied Using Nanoparticles in Living Endothelial Cells. *ACS Nano* **2009**, *3* (12), 4110−4116.

(43) Wang, Z.; et al. Delivery of nanoparticle: complexed drugs across the vascular endothelial barrier via caveolae. *IUBMB Life* **2011**, *63* (8), 659−667.

(44) Ye, D.; et al. Nanoparticle accumulation and transcytosis in brain endothelial cell layers. *Nanoscale* **2013**, *5* (22), 11153−11165.

(45) Balklava, Z.; et al. Genome-wide analysis identifies a general requirement for polarity proteins in endocytic traffic. *Nat. Cell Biol.* **2007**, *9* (9), 1066−1073.

(46) Shivas, J. M.; et al. Polarity and endocytosis: reciprocal regulation. *Trends Cell Biol.* **2010**, *20* (8), 445−452.

(47) Rao, Y.; Haucke, V. Membrane shaping by the Bin/amphiphysin/Rvs (BAR) domain protein superfamily. *Cell. Mol. Life Sci.* **2011**, *68*, 3983−3993.

(48) Grant, B. D.; Donaldson, J. G. Pathways and mechanisms of endocytic recycling. *Nat. Rev. Mol. Cell Biol.* **2009**, *10* (9), 597−608.

(49) Summers, B. D.; et al. Lung lymphatic thrombosis and dysfunction caused by cigarette smoke exposure precedes emphysema in mice. *Sci. Rep.* **2022**, *12* (1), 5012.

(50) Randolph, G. J.; et al. Lymphoid Aggregates Remodel Lymphatic Collecting Vessels that Serve Mesenteric Lymph Nodes in Crohn Disease. *Am. J. Pathol.* **2016**, *186* (12), 3066−3073.

(51) Ivanov, S.; et al. CCR7 and IRF4-dependent dendritic cells regulate lymphatic collecting vessel permeability. *J. Clin. Invest.* **2016**, *126* (4), 1581−1591.

(52) Jannaway, M.; Scallan, J. P. VE-Cadherin and Vesicles Differentially Regulate Lymphatic Vascular Permeability to Solutes of Various Sizes. *Front. Physiol.* **2021**, *12*, No. 687563.

(53) Yamaji, Y.; et al. Development of a mouse model for the visual and quantitative assessment of lymphatic trafficking and function by in vivo imaging. *Sci. Rep.* **2018**, *8* (1), 5921.

(54) Savetsky, I. L.; et al. Th2 cytokines inhibit lymphangiogenesis. *PLoS One* **2015**, *10* (6), No. e0126908.

(55) Churchill, M. J.; et al. Infection-induced lymphatic zippering restricts fluid transport and viral dissemination from skin. *J. Exp. Med.* **2022**, *219* (5), No. e20211830.

(56) Kataru, R. P.; et al. Regulation of Immune Function by the Lymphatic System in Lymphedema. *Front. Immunol.* **2019**, *10*, 470.

(57) Kataru, R. P.; et al. Fibrosis and secondary lymphedema: chicken or egg? *Transl. Res.* **2019**, *209*, 68−76.

(58) Czepielewski, R. S.; et al. Ileitis-associated tertiary lymphoid organs arise at lymphatic valves and impede mesenteric lymph flow in response to tumor necrosis factor. *Immunity* **2021**, *54* (12), 2795−2811.e9.

(59) Levenberg, K. A method for the solution of certain non-linear problems in least squares. *Quart. Appl. Math.* **1944**, *2* (2), 164−168.

(60) Chou, W.-C.; et al. Development of a multi-route physiologically based pharmacokinetic (PBPK) model for nanomaterials: a comparison between a traditional versus a new route-specific approach using gold nanoparticles in rats. *Part. Fibre Toxicol.* **2022**, *19* (1), 47.

(61) Glass, E. M.; et al. Multiphysics pharmacokinetic model for targeted nanoparticles. *Front. Med. Technol.* **2022**, *4*, No. 934015.

(62) Sousa-Junior, A.; et al. A Predictive Pharmacokinetic Model for Immune Cell-Mediated Uptake and Retention of Nanoparticles in Tumors. *Int. J. Mol. Sci.* **2022**, *23*, 15664.

(63) Neubauer, A. M.; et al. Nanoparticle pharmacokinetic profiling in vivo using magnetic resonance imaging. *Magn. Reson. Med.* **2008**, *60* (6), 1353−1361.

(64) Georgieva, J. V.; et al. Surface Characteristics of Nanoparticles Determine Their Intracellular Fate in and Processing by Human Blood−Brain Barrier Endothelial Cells In Vitro. *Mol. Ther.* **2011**, *19* (2), 318−325.

(65) Fiorentino, I.; et al. Energy independent uptake and release of polystyrene nanoparticles in primary mammalian cell cultures. *Exp. Cell Res.* **2015**, *330* (2), 240−247.

(66) Firdessa, R.; Oelschlaeger, T. A.; Moll, H. Identification of multiple cellular uptake pathways of polystyrene nanoparticles and factors affecting the uptake: Relevance for drug delivery systems. *Eur. J. Cell Biol.* **2014**, *93* (8), 323−337.

(67) Fazlollahi, F.; et al. Polystyrene nanoparticle trafficking across MDCK-II. *Nanomedicine* **2011**, *7* (5), 588−594.

(68) Yacobi, N. R.; et al. Mechanisms of Alveolar Epithelial Translocation of a Defined Population of Nanoparticles. *Am. J. Respir. Cell Mol. Biol.* **2010**, *42* (5), 604−614.

(69) Rappoport, J.; et al. Cellular entry of nanoparticles via serum sensitive clathrin-mediated endocytosis, and plasma membrane permeabilization. *Int. J. Nanomed.* **2012**, *7*, 2045.